SIAM J. SCI. COMPUT.
Vol. 38, No. 1, pp. A105–A127

LOCAL DISCONTINUOUS GALERKIN METHOD AND HIGH ORDER SEMI-IMPLICIT SCHEME FOR THE PHASE FIELD CRYSTAL EQUATION*

RUIHAN GUO† AND YAN XU‡

Abstract. In this paper, we present a local discontinuous Galerkin (LDG) method and two unconditionally energy stable schemes for the phase field crystal (PFC) equation. The semidiscrete energy stability of the LDG method is proved first. The PFC equation is a sixth order nonlinear partial differential equation (PDE), which leads to the severe time step restriction ($\Delta t = \mathcal{O}(\Delta x^6)$) of explicit time discretization methods to maintain stability. Due to this, we introduce semi-implicit first order and second order time discretization methods which are based on the convex splitting principle of a discrete energy and prove the corresponding unconditional energy stabilities. To improve the temporal accuracy, the spectral deferred correction (SDC) method and a high order semi-implicit Runge–Kutta method combining with the first–order convex splitting method are adopted for the PFC equation with constant and degenerate mobility, respectively. The equations at the implicit time level are nonlinear and we employ an efficient nonlinear multigrid solver to solve the equations. In particular, we show the multigrid solver has optimal complexity numerically. Numerical results are also given to illustrate that the combination of the LDG method for spatial approximation, SDC, and high order semi-implicit time marching methods with the multigrid solver provides an efficient and practical approach when solving the PFC equation.

Key words. phase field crystal equation, local discontinuous Galerkin method, energy stability, convex splitting, spectral deferred correction, semi-implicit Runge–Kutta method, multigrid

AMS subject classifications. 65M60, 35Q82

DOI. 10.1137/15M1038803

1. Introduction.

In this paper, we consider numerical methods in a bounded domain $\Omega \in \mathbb{R}^d (d \leq 3)$ for the phase field crystal (PFC) equation:

$$\phi_t = \nabla \cdot (M(\phi) \nabla \mu), \tag{1.1}$$

where $M(\phi) \geq 0$ is a mobility, and μ is the chemical potential defined as

$$\mu := \phi^3 + (1 - \epsilon)\phi + 2\Delta\phi + \Delta^2\phi. \tag{1.2}$$

Various unconditionally stable first order and second order temporal discretization schemes coupled with finite difference methods [11, 16] and finite element methods [10] have been developed for the PFC equation recently. Usually only second order spatial accuracy was achieved for both finite difference and finite element methods. The goal of this paper is to develop a local discontinuous Galerkin (LDG) method for the general nonlinear PFC equation. Our proposed LDG scheme is high order accurate, nonlinear stable, and flexible for arbitrary h and p adaptivity, and we also prove the energy stability of the semidiscrete LDG scheme for the PFC equation.

*Submitted to the journal's Methods and Algorithms for Scientific Computing section September 10, 2015; accepted for publication (in revised form) November 18, 2015; published electronically January 6, 2016.

http://www.siam.org/journals/sisc/38-1/M103880.html

†Institut Camille Jordan, Université Claude Bernard Lyon I, 43 boulevard 11 novembre 1918, 69622 Villeurbanne cedex, France (rguo@math.univ-lyon1.fr).

‡Corresponding author. School of Mathematical Sciences, University of Science and Technology of China, Hefei, Anhui 230026, People Republic of China (yxu@ustc.edu.cn). This author's work was supported by NSFC grants 11371342, 11426236.

The discontinuous Galerkin (DG) method we discuss in this paper is a class of finite element methods, using discontinuous, piecewise polynomials as the solution and test spaces. Reed and Hill [14] first developed the DG method in 1973, in the framework of neutron linear transport equation. Later, Cockburn and others [3, 4, 5, 6] applied the DG method for solving a series of nonlinear hyperbolic equations. It is difficult to apply the DG method directly for partial differential equations (PDEs) containing higher order spatial derivatives; therefore the LDG method was introduced. The main idea of the LDG method is to rewrite the equations with higher order derivatives as a first order system, then apply the DG method to the system, in which choosing proper numerical fluxes is the key ingredient to ensure stability. For a detailed description about the LDG methods for high order time-dependent PDEs, we refer readers to the review paper [19]. A common feature of these LDG methods is that stability can be proved for quite general nonlinear cases. DG and LDG methods also have several attractive properties, such as their flexibility for general geometry, unstructured meshes, arbitrary h and p adaptivity, and their excellent parallel efficiency.

For PDEs containing higher order spatial derivatives, explicit time discretization methods will suffer from an extremely small time step restriction for stability, but not for accuracy. The PFC equation itself experiences long time evolution; therefore computational efficiency is essential to map out the whole dynamics from initial state to steady state. It would therefore be desirable to develop implicit or semi-implicit time discretization techniques to alleviate this problem. The first and second order unconditionally energy stable finite difference schemes for PFC equation were developed based on the convex splitting principle of a discrete energy in [16, 11]. Unfortunately, these convex splitting schemes are only first or second order accurate in temporal accuracy and second order accurate in spatial accuracy, and they are not easy to extend to higher order accuracy in both time and space.

In this paper, we present the semi-implicit SDC method coupled with the convex splitting scheme to obtain high order temporal accuracy for PFC equation with constant mobility. For the PFC equation with degenerate mobility, the application of the SDC method will result in fully implicit schemes, which increases the difficulty of implementation. In addition, it is difficult to separate the stiff and nonstiff components in this case, which leads to the uselessness of traditional implicit-explicit methods. We present a high order semi-implicit Runge–Kutta scheme which was proposed by Boscarino, Filbet, and Russo, [1] combining with the convex splitting scheme to achieve high order temporal accuracy. Numerical experiments are given to validate that with the proposed schemes, we can obtain high order accuracy in both time and space.

The organization of the paper is as follows. In section 2, we review the properties of the PFC equation. In section 3, we present an LDG method for the PFC equation and prove the semidiscrete energy stability. In section 4, we first present the first order and second order convex splitting schemes coupled with LDG spatial discretization and prove the corresponding unconditional energy stabilities for the fully discrete schemes. Then, the semi-implicit SDC method and a high order semi-implicit method combining with the first order convex splitting are introduced to achieve high order temporal accuracy for the PFC equation with constant and degenerate mobility, respectively. Section 5 contains numerical results for the nonlinear PFC equation, which demonstrate the accuracy and capability of the LDG method, the temporal discretization methods, and the multigrid solver. Finally, we give concluding remarks in section 6.

2. The PFC equation. The PFC model was recently proposed by Elder et al. [8, 9] to study the nonequilibrium microstructure formation by introducing a free energy functional of the local-time-averaged density field. In the PFC model, a phase field formulation is introduced that accounts for the periodic structure of a crystal lattice through a free energy functional of Swift–Hohenberg type [15] that is minimized by periodic functions. The model can account for elastic and plastic deformations of the lattice, dislocations, grain boundaries, and many other observable phenomena, which was proposed by Provatas et al. [13] in a recent review.

We consider a dimensionless energy of the form [8, 15]

$$E(\phi) = \int_\Omega \left\{ \frac{1}{4}\phi^4 + \frac{1-\epsilon}{2}\phi^2 - |\nabla\phi|^2 + \frac{1}{2}(\Delta\phi)^2 \right\} d\boldsymbol{x}, \tag{2.1}$$

where $\Omega \subset \mathbb{R}^d$, $d = 2$ or 3, $\phi : \Omega \to \mathbb{R}$ is the density field, and ϵ is a constant. For simplicity, let us assume that $\Omega = (0, L_x) \times (0, L_y)$ and that ϕ and $\Delta\phi$ are periodic on $\partial\Omega$.

The Euler–Lagrangian variation with respect to ϕ gives the chemical potential

$$\mu := \frac{\delta E}{\delta \phi} = \phi^3 + (1-\epsilon)\phi + 2\Delta\phi + \Delta^2\phi. \tag{2.2}$$

We consider two types of gradient dynamics on Ω: (i) nonconserved dynamics,

$$\phi_t = -M(\phi)\mu, \tag{2.3}$$

where $M(\phi) \geq 0$ is a mobility, and (ii) conserved dynamics,

$$\phi_t = \nabla \cdot (M(\phi)\nabla\mu). \tag{2.4}$$

For the conserved dynamics equation, we assume that μ is periodic on $\partial\Omega$. The gradient flow (2.4) is mass preserving and the total energy decays with respect to time t, i.e.,

$$\begin{aligned} \frac{d}{dt}E &= \int_\Omega \{\phi^3\phi_t + (1-\epsilon)\phi\phi_t - 2\nabla\phi\cdot\nabla\phi_t + \Delta\phi\Delta\phi_t\} d\boldsymbol{x} \\ &= \int_\Omega \{\phi^3 + (1-\epsilon)\phi + 2\Delta\phi + \Delta^2\phi\}\phi_t d\boldsymbol{x} \\ &= \int_\Omega \mu\nabla\cdot(M(\phi)\nabla\mu) d\boldsymbol{x} = -\int_\Omega M(\phi)\nabla\mu\cdot\nabla\mu d\boldsymbol{x} \leq 0. \end{aligned}$$

The fourth order equation (2.3) is the Swift–Hohenberg equation [15], which is nonconserved. The PFC equation (2.4) is a conservative form of the Swift–Hohenberg equation (2.3). What we should keep in mind is that the dynamics described by (2.3) and (2.4) are different. In this paper, we just focus on the PFC equation and design an LDG method and unconditionally stable time marching methods such that relatively large time steps can be used for numerical simulations.

3. The LDG method for the PFC equation. In this subsection, we develop an LDG method for the PFC equation in $\Omega \in \mathbb{R}^d$ with $d \leq 3$. Although we do not address numerical experiments in three dimensions in this paper, the LDG method and the energy stability results of this paper are valid for all $d \leq 3$.

3.1. Notation. Let $\mathcal{T}_h$ denote a tessellation of Ω with shape-regular elements K. Let Γ denote the union of the boundary faces of elements $K \in \mathcal{T}_h$, i.e., $\Gamma = \cup_{K\in\mathcal{T}_h}\partial K$, and $\Gamma_0 = \Gamma\backslash\partial\Omega$. In order to describe the flux functions, we need to introduce some notation. Let e be a face shared by the "left" and "right" elements K_L and K_R. For our purpose "left" and "right" can be uniquely defined for each face according to any fixed rule; see, e.g., [19, 20] for more details of such a definition. Define the normal vectors $\boldsymbol{\nu}_L$ and $\boldsymbol{\nu}_R$ on e pointing exterior to K_L and K_R, respectively. If ψ is a function on K_L and K_R, but possibly discontinuous across e, let ψ_L denote $(\psi|_{K_L})|_e$ and ψ_R denote $(\psi|_{K_R})|_e$, the left and right trace, respectively.

Let $\mathcal{P}^k(K)$ be the space of polynomials of degree at most $k \geq 0$ on $K \in \mathcal{T}_h$. The finite element spaces are denoted by

$$V_h = \Big\{\varphi : \quad \varphi|_K \in \mathcal{P}^k(K) \quad \forall K \in \mathcal{T}_h\Big\},$$
$$\Sigma_h^d = \Big\{\Phi = (\phi_1, \ldots, \phi_d)^T : \quad \phi_l|_K \in \mathcal{P}^k(K), \ \ l = 1\cdots d, \quad \forall K \in \mathcal{T}_h\Big\}.$$

Note that functions in V_h, Σ_h^d are allowed to be completely discontinuous across element interfaces.

3.2. The LDG method. To construct the LDG method, first we rewrite the PFC equation (2.4) as a system containing only first order derivatives:

$$\phi_t = \nabla\cdot\boldsymbol{p}, \tag{3.1a}$$
$$\boldsymbol{p} = M(\phi)\boldsymbol{s}, \tag{3.1b}$$
$$\boldsymbol{s} = \nabla(r + 2q + q_2), \tag{3.1c}$$
$$q_2 = \nabla\cdot\boldsymbol{q}_1, \tag{3.1d}$$
$$\boldsymbol{q}_1 = \nabla q, \tag{3.1e}$$
$$q = \nabla\cdot\boldsymbol{w}, \tag{3.1f}$$
$$\boldsymbol{w} = \nabla\phi, \tag{3.1g}$$
$$r = \phi^3 + (1-\epsilon)\phi. \tag{3.1h}$$

To simplify the notation, we still use ϕ, $\boldsymbol{p}$, $\boldsymbol{s}$, q_2, $\boldsymbol{q}_1$, q, $\boldsymbol{w}$, and r to denote the numerical solution. The LDG scheme to solve the system (3.1) is as follows: Find ϕ, q_2, q, $r \in V_h$, and $\boldsymbol{p}$, $\boldsymbol{s}$, $\boldsymbol{q}_1$, $\boldsymbol{w} \in \Sigma_h^d$, such that, for all test functions φ_1, φ_2, φ_3, $\varphi_4 \in V_h$, and $\boldsymbol{\theta}_1$, $\boldsymbol{\theta}_2$, $\boldsymbol{\theta}_3$, $\boldsymbol{\theta}_4 \in \Sigma_h^d$, we have

$$\int_K \phi_t\varphi_1 dK = -\int_K \boldsymbol{p}\cdot\nabla\varphi_1 dK + \int_{\partial K}\widehat{\boldsymbol{p}}\cdot\boldsymbol{\nu}\varphi_1 ds, \tag{3.2a}$$
$$\int_K \boldsymbol{p}\cdot\boldsymbol{\theta}_1 dK = \int_K M(\phi)\boldsymbol{s}\cdot\boldsymbol{\theta}_1 dK, \tag{3.2b}$$
$$\int_K \boldsymbol{s}\cdot\boldsymbol{\theta}_2 dK = -\int_K (r+2q+q_2)\nabla\cdot\boldsymbol{\theta}_2 dK + \int_{\partial K}(\widehat{r}+2\widehat{q}+\widehat{q_2})\boldsymbol{\theta}_2\cdot\boldsymbol{\nu} ds, \tag{3.2c}$$
$$\int_K q_2\varphi_2 dK = -\int_K \boldsymbol{q}_1\cdot\nabla\varphi_2 dK + \int_{\partial K}\widehat{\boldsymbol{q}}_1\cdot\boldsymbol{\nu}\varphi_2 ds, \tag{3.2d}$$
$$\int_K \boldsymbol{q}_1\cdot\boldsymbol{\theta}_3 dK = -\int_K q\nabla\cdot\boldsymbol{\theta}_3 dK + \int_{\partial K}\widehat{q}\boldsymbol{\theta}_3\cdot\boldsymbol{\nu} ds, \tag{3.2e}$$
$$\int_K q\varphi_3 dK = -\int_K \boldsymbol{w}\cdot\nabla\varphi_3 dK + \int_{\partial K}\widehat{\boldsymbol{w}}\cdot\boldsymbol{\nu}\varphi_3 ds, \tag{3.2f}$$

$$\int_K \boldsymbol{w}\cdot\boldsymbol{\theta}_4 dK = -\int_K \phi\nabla\cdot\boldsymbol{\theta}_4 dK + \int_{\partial K}\widehat{\phi}\boldsymbol{\theta}_4\cdot\boldsymbol{\nu}ds, \tag{3.2g}$$

$$\int_K r\varphi_4 dK = \int_K (\phi^3 + (1-\epsilon)\phi)\varphi_4 dK. \tag{3.2h}$$

The "hat" terms in (3.2) in the cell boundary terms from integration by parts are the so-called numerical fluxes, which are functions defined on the edges and should be designed based on different guiding principles for different PDEs to ensure stability and local solvability of the intermediate variables. It turns out that we can take the simple choices such as

$$\widehat{\boldsymbol{p}}|_e = \boldsymbol{p}_R,\quad \widehat{r}|_e = r_L,\quad \widehat{q}_2|_e = q_{2L},\quad \widehat{\boldsymbol{q}}_1|_e = \boldsymbol{q}_{1R},\quad \widehat{q}|_e = q_L,\quad \widehat{\boldsymbol{w}}|_e = \boldsymbol{w}_R,\quad \widehat{\phi}|_{e=\phi_L}. \tag{3.3}$$

We remark that the choice for the fluxes (3.3) is not unique. Considering the compactness of the stencil and the optimal accuracy, the crucial part is taking $\widehat{r}$, $\widehat{q}_2$, $\widehat{q}$, and $\widehat{\boldsymbol{p}}$ from opposite sides, $\widehat{\boldsymbol{q}}_1$ and $\widehat{\phi}$ from opposite sides, and $\widehat{\boldsymbol{w}}$ and $\widehat{q}$ from opposite sides, $\widehat{\boldsymbol{w}}$ and $\widehat{\phi}$ from opposite sides.

3.3. Energy dissipative. It is easy to show that the LDG scheme is mass conservative. We also can prove the semidiscrete scheme is energy stable in the following.

PROPOSITION 3.1 (energy stability for the semidiscrete LDG scheme). *The solution to the LDG scheme* (3.2) *with the flux* (3.3) *satisfies the energy dissipative*

$$\frac{d}{dt}\int_\Omega \left(\frac{1}{4}\phi^4 + \frac{1-\epsilon}{2}\phi^2 - \boldsymbol{w}\cdot\boldsymbol{w} + \frac{1}{2}q^2\right)d\boldsymbol{x} \le 0. \tag{3.4}$$

Proof. First, we take the time derivative of (3.2g) and choose the test functions $\boldsymbol{\theta}_4 = -2\boldsymbol{w}$, $-\boldsymbol{q}_1$ separately to obtain

$$-2\int_K \boldsymbol{w}_t\cdot\boldsymbol{w}dK = 2\int_K \phi_t\nabla\cdot\boldsymbol{w}dK - 2\int_{\partial K}\widehat{\phi}_t\boldsymbol{w}\cdot\boldsymbol{\nu}ds, \tag{3.5}$$

$$-\int_K \boldsymbol{w}_t\cdot\boldsymbol{q}_1 dK = \int_K \phi_t\nabla\cdot\boldsymbol{q}_1 dK - \int_{\partial K}\widehat{\phi}_t\boldsymbol{q}_1\cdot\boldsymbol{\nu}ds. \tag{3.6}$$

Then we take the time derivative of (3.2f) and choose the test function $\varphi_3 = q$ to get

$$\int_K q_t q dK = -\int_K \boldsymbol{w}_t\cdot\nabla q dK + \int_{\partial K}\widehat{\boldsymbol{w}}_t\cdot\boldsymbol{\nu}q ds. \tag{3.7}$$

For other equations in scheme (3.2), we choose the test functions

$$\varphi_1 = r + 2q + q_2,\ \boldsymbol{\theta}_1 = -\boldsymbol{s},\ \boldsymbol{\theta}_2 = \boldsymbol{p},\ \varphi_2 = -\phi_t,\ \boldsymbol{\theta}_3 = \boldsymbol{w}_t,\ \varphi_3 = -2\phi_t,\ \varphi_4 = -\phi_t,$$

respectively, to get

$$\int_K \phi_t(r+2q+q_2)dK = -\int_K \boldsymbol{p}\cdot\nabla(r+2q+q_2)dK + \int_{\partial K}\widehat{\boldsymbol{p}}\cdot\boldsymbol{\nu}(r+2q+q_2)ds,$$

$$-\int_K \boldsymbol{p}\cdot\boldsymbol{s}dK = -\int_K M(\phi)\boldsymbol{s}\cdot\boldsymbol{s}dK,$$

$$\int_K \boldsymbol{s}\cdot\boldsymbol{p}dK = -\int_K (r+2q+q_2)\nabla\cdot\boldsymbol{p}dK + \int_{\partial K}(\widehat{r}+2\widehat{q}+\widehat{q}_2)\boldsymbol{p}\cdot\boldsymbol{\nu}ds,$$
$$-\int_K q_2\phi_t dK = \int_K \boldsymbol{q}_1\cdot\nabla\phi_t dK - \int_{\partial K}\widehat{\boldsymbol{q}}_1\cdot\boldsymbol{\nu}\phi_t ds,$$
$$\int_K \boldsymbol{q}_1\cdot\boldsymbol{w}_t dK = -\int_K q\nabla\cdot\boldsymbol{w}_t dK + \int_{\partial K}\widehat{q}\boldsymbol{w}_t\cdot\boldsymbol{\nu}ds,$$
$$-2\int_K q\phi_t dK = 2\int_K \boldsymbol{w}\cdot\nabla\phi_t dK - 2\int_{\partial K}\widehat{\boldsymbol{w}}\cdot\boldsymbol{\nu}\phi_t ds,$$
$$-\int_K r\phi_t dK = -\int_K (\phi^3+(1-\epsilon)\phi)\phi_t dK.$$

Combining the above equations with (3.5)–(3.7), we find

$$\begin{aligned}(3.8)\quad &\frac{d}{dt}\int_K\left(\frac{1}{4}\phi^4+\frac{1-\epsilon}{2}\phi^2-\boldsymbol{w}\cdot\boldsymbol{w}+\frac{1}{2}q^2\right)dK+\int_K M(\phi)\boldsymbol{s}\cdot\boldsymbol{s}dK\\ &=-\int_K\nabla\cdot((r+2q+q_2)\boldsymbol{p})dK+\int_{\partial K}(\widehat{\boldsymbol{p}}\cdot\boldsymbol{\nu}(r+2q+q_2)+(\widehat{r}+2\widehat{q}+\widehat{q}_2)\boldsymbol{p}\cdot\boldsymbol{\nu})ds\\ &\quad+\int_K\nabla\cdot(\phi_t\boldsymbol{q}_1)dK-\int_{\partial K}(\widehat{\phi}_t\boldsymbol{q}_1\cdot\boldsymbol{\nu}+\widehat{\boldsymbol{q}}_1\cdot\boldsymbol{\nu}\phi_t)ds\\ &\quad-\int_K\nabla\cdot(q\boldsymbol{w}_t)dK+\int_{\partial K}(\widehat{\boldsymbol{w}}_t\cdot\boldsymbol{\nu}q+\widehat{q}\boldsymbol{w}_t\cdot\boldsymbol{\nu})ds\\ &\quad+2\int_K\nabla\cdot(\phi_t\boldsymbol{w})dK-2\int_{\partial K}(\widehat{\phi}_t\boldsymbol{w}\cdot\boldsymbol{\nu}+\widehat{\boldsymbol{w}}\cdot\boldsymbol{\nu}\phi_t)ds.\end{aligned}$$

Finally, summing up (3.8) over K and noticing the fluxes in (3.3) are from the opposite sides of ∂K as well as the periodic boundary conditions, we have

$$\frac{d}{dt}\int_K\left(\frac{1}{4}\phi^4+\frac{1-\epsilon}{2}\phi^2-\boldsymbol{w}\cdot\boldsymbol{w}+\frac{1}{2}q^2\right)dK+\int_K M(\phi)\boldsymbol{s}\cdot\boldsymbol{s}dK=0,$$

which implies the energy dissipative result (3.4). ∎

4. Time discretization. The LDG spatial discretization for the PFC equation typically results in an ordinary differential equation (ODE). The PFC equation is a sixth order nonlinear PDE and explicit time marching methods usually require a severe time step ($\Delta t = \mathcal{O}(\Delta x^6)$) restriction for stability, and it itself experiences a long time evolution from initial state to steady state, which leads to explicit methods being nearly useless. Therefore, we will devote ourselves to exploring semi-implicit time marching methods to relax this constraint of the time step.

4.1. First order convex splitting scheme. Wise and others [16, 11] introduced an unconditionally stable finite difference scheme for the PFC equation based on a convex splitting of the discrete energy. Based on the work in [16, 11], we apply the convex splitting method to the PFC equation coupled with the LDG spatial discretization and obtain an unconditionally stable fully discrete scheme. The corresponding convex splitting scheme is given as follows:

$$\frac{\phi^{n+1}-\phi^n}{\Delta t} = \nabla\cdot(M(\phi^n)\nabla\mu^{n+1}), \tag{4.1a}$$
$$\mu^{n+1} = (\phi^{n+1})^3+(1-\epsilon)\phi^{n+1}+2\Delta\phi^n+\Delta^2\phi^{n+1}. \tag{4.1b}$$

The LDG scheme to solve the convex splitting scheme (4.1) becomes the following: Find ϕ^{n+1}, q_2^{n+1}, q^{n+1}, $r^{n+1} \in V_h$ and $\boldsymbol{p}^{n+1}$, $\boldsymbol{s}^{n+1}$, $\boldsymbol{q}_1^{n+1}$, $\boldsymbol{w}^{n+1} \in \Sigma_h^d$ such that, for all test functions φ_1, φ_2, φ_3, $\varphi_4 \in V_h$ and $\boldsymbol{\theta}_1$, $\boldsymbol{\theta}_2$, $\boldsymbol{\theta}_3$, $\boldsymbol{\theta}_4 \in \Sigma_h^d$, we have

$$\int_K \frac{\phi^{n+1}-\phi^n}{\Delta t}\varphi_1 dK = -\int_K \boldsymbol{p}^{n+1}\cdot\nabla\varphi_1 dK + \int_{\partial K}\widehat{\boldsymbol{p}}^{n+1}\cdot\boldsymbol{\nu}\varphi_1 ds, \tag{4.2a}$$

$$\int_K \boldsymbol{p}^{n+1}\cdot\boldsymbol{\theta}_1 dK = \int_K M(\phi^n)\boldsymbol{s}^{n+1}\cdot\boldsymbol{\theta}_1 dK, \tag{4.2b}$$

$$\begin{aligned}\int_K \boldsymbol{s}^{n+1}\cdot\boldsymbol{\theta}_2 dK = &-\int_K (r^{n+1}+2q^n+q_2^{n+1})\nabla\cdot\boldsymbol{\theta}_2 dK\\ &+\int_{\partial K}(\widehat{r}^{n+1}+2\widehat{q}^n+\widehat{q}_2^{n+1})\boldsymbol{\theta}_2\cdot\boldsymbol{\nu} ds,\end{aligned} \tag{4.2c}$$

$$\int_K q_2^{n+1}\varphi_2 dK = -\int_K \boldsymbol{q}_1^{n+1}\cdot\nabla\varphi_2 dK + \int_{\partial K}\widehat{\boldsymbol{q}}_1^{n+1}\cdot\boldsymbol{\nu}\varphi_2 ds, \tag{4.2d}$$

$$\int_K \boldsymbol{q}_1^{n+1}\cdot\boldsymbol{\theta}_3 dK = -\int_K q^{n+1}\nabla\cdot\boldsymbol{\theta}_3 dK + \int_{\partial K}\widehat{q}^{n+1}\boldsymbol{\theta}_3\cdot\boldsymbol{\nu} ds, \tag{4.2e}$$

$$\int_K q^{n+1}\varphi_3 dK = -\int_K \boldsymbol{w}^{n+1}\cdot\nabla\varphi_3 dK + \int_{\partial K}\widehat{\boldsymbol{w}}^{n+1}\cdot\boldsymbol{\nu}\varphi_3 ds, \tag{4.2f}$$

$$\int_K \boldsymbol{w}^{n+1}\cdot\boldsymbol{\theta}_4 dK = -\int_K \phi^{n+1}\nabla\cdot\boldsymbol{\theta}_4 dK + \int_{\partial K}\widehat{\phi}^{n+1}\boldsymbol{\theta}_4\cdot\boldsymbol{\nu} ds, \tag{4.2g}$$

$$\int_K r^{n+1}\varphi_4 dK = \int_K ((\phi^{n+1})^3 + (1-\epsilon)\phi^{n+1})\varphi_4 dK. \tag{4.2h}$$

The numerical fluxes are

$$\begin{aligned}&\widehat{\boldsymbol{p}}^{n+1}|_e = \boldsymbol{p}_R^{n+1}, \quad \widehat{r}^{n+1}|_e = r_L^{n+1}, \quad \widehat{q}_2^{n+1}|_e = q_{2L}^{n+1}, \quad \widehat{\boldsymbol{q}}_1^{n+1}|_e = \boldsymbol{q}_{1R}^{n+1},\\ &\widehat{q}^{n+1}|_e = q_L^{n+1}, \quad \widehat{\boldsymbol{w}}^{n+1}|_e = \boldsymbol{w}_R^{n+1}, \quad \widehat{\phi}^{n+1}|_e = \phi_L^{n+1}.\end{aligned} \tag{4.3}$$

Next, we will prove the unconditional discrete energy stability for the fully discrete LDG scheme (4.2). To simplify the notation, we use the following notation for discretization of time variable:

$$\begin{aligned}\delta_t\phi^{n+1} &= \frac{\phi^{n+1}-\phi^n}{\Delta t},\\ \delta_t\boldsymbol{w}^{n+1} &= \frac{\boldsymbol{w}^{n+1}-\boldsymbol{w}^n}{\Delta t},\\ \delta_t q^{n+1} &= \frac{q^{n+1}-q^n}{\Delta t}.\end{aligned}$$

Proposition 4.1 (energy stability for the fully discrete LDG scheme with first order convex splitting scheme). *The solution to the LDG scheme* (4.2) *with the flux* (4.3) *satisfies the discrete energy dissipative*

$$\begin{aligned}&\frac{1}{\Delta t}\left[\int_\Omega\left(\frac{1}{2}(q^{n+1})^2-\boldsymbol{w}^{n+1}\cdot\boldsymbol{w}^{n+1}+\frac{1}{4}(\phi^{n+1})^4+\frac{1-\epsilon}{2}(\phi^{n+1})^2\right)d\boldsymbol{x}\right]\\ &\quad+\int_\Omega M(\phi^n)\boldsymbol{s}^{n+1}\cdot\boldsymbol{s}^{n+1}d\boldsymbol{x}\\ &\le\frac{1}{\Delta t}\left[\int_\Omega\left(\frac{1}{2}(q^n)^2-\boldsymbol{w}^n\cdot\boldsymbol{w}^n+\frac{1}{4}(\phi^n)^4+\frac{1-\epsilon}{2}(\phi^n)^2\right)d\boldsymbol{x}\right].\end{aligned}$$

Proof. For (4.2), choosing the test functions

$$\varphi_1 = r^{n+1} + 2q^n + q_2^{n+1}, \quad \boldsymbol{\theta}_1 = -\boldsymbol{s}^{n+1}, \quad \boldsymbol{\theta}_2 = \boldsymbol{p}^{n+1}, \quad \varphi_2 = -\delta_t\phi^{n+1},$$
$$\boldsymbol{\theta}_3 = \delta_t\boldsymbol{w}^{n+1}, \quad \varphi_3 = \delta_t q^{n+1}, \quad \boldsymbol{\theta}_4 = -\frac{1}{\Delta t}\boldsymbol{q}_1^{n+1}, \quad \varphi_4 = -\delta_t\phi^{n+1},$$

we get

$$\begin{aligned}
\int_K \delta_t\phi^{n+1}(r^{n+1} + 2q^n + q_2^{n+1})dK =& -\int_K \boldsymbol{p}^{n+1}\cdot\nabla(r^{n+1} + 2q^n + q_2^{n+1})dK \\
&+ \int_{\partial K} \widehat{\boldsymbol{p}}^{n+1}\cdot\boldsymbol{\nu}(r^{n+1} + 2q^n + q_2^{n+1})ds, \\
-\int_K \boldsymbol{p}^{n+1}\cdot\boldsymbol{s}^{n+1}dK =& -\int_K M(\phi^n)\boldsymbol{s}^{n+1}\cdot\boldsymbol{s}^{n+1}dK, \\
\int_K \boldsymbol{s}^{n+1}\cdot\boldsymbol{p}^{n+1}dK =& -\int_K (r^{n+1} + 2q^n + q_2^{n+1})\nabla\cdot\boldsymbol{p}^{n+1}dK \\
&+ \int_{\partial K} (\widehat{r}^{n+1} + 2\widehat{q}^n + \widehat{q}_2^{n+1})\boldsymbol{p}^{n+1}\cdot\boldsymbol{\nu}ds, \\
-\int_K q_2^{n+1}\delta_t\phi^{n+1}dK =& \int_K \boldsymbol{q}_1^{n+1}\cdot\nabla\delta_t\phi^{n+1}dK - \int_{\partial K}\widehat{\boldsymbol{q}}_1^{n+1}\cdot\boldsymbol{\nu}\delta_t\phi^{n+1}ds, \\
\int_K \boldsymbol{q}_1^{n+1}\cdot\delta_t\boldsymbol{w}^{n+1}dK =& -\int_K q^{n+1}\nabla\cdot\delta_t\boldsymbol{w}^{n+1}dK + \int_{\partial K}\widehat{q}^{n+1}\delta_t\boldsymbol{w}^{n+1}\cdot\boldsymbol{\nu}ds, \\
\int_K q^{n+1}\delta_t q^{n+1}dK =& -\int_K \boldsymbol{w}^{n+1}\cdot\nabla\delta_t q^{n+1}dK + \int_{\partial K}\widehat{\boldsymbol{w}}^{n+1}\cdot\boldsymbol{\nu}\delta_t q^{n+1}ds, \\
-\frac{1}{\Delta t}\int_K \boldsymbol{w}^{n+1}\cdot\boldsymbol{q}_1^{n+1}dK =& \frac{1}{\Delta t}\int_K \phi^{n+1}\nabla\cdot\boldsymbol{q}_1^{n+1}dK - \frac{1}{\Delta t}\int_{\partial K}\widehat{\phi}^{n+1}\boldsymbol{q}_1^{n+1}\cdot\boldsymbol{\nu}ds, \\
-\int_K r^{n+1}\delta_t\phi^{n+1}dK =& -\int_K ((\phi^{n+1})^3 + (1-\epsilon)\phi^{n+1})\delta_t\phi^{n+1}dK.
\end{aligned} \tag{4.4}$$

By (4.2f), at time level t^n, we have

$$\int_K q^n\varphi_3 dK = -\int_K \boldsymbol{w}^n\cdot\nabla\varphi_3 dK + \int_{\partial K}\widehat{\boldsymbol{w}}^n\cdot\boldsymbol{\nu}\varphi_3 ds. \tag{4.5}$$

Choosing the test function $\varphi_3 = -2\delta_t\phi^{n+1}$ in (4.5), we obtain

$$-2\int_K q^n\delta_t\phi^{n+1}dK = 2\int_K \boldsymbol{w}^n\cdot\nabla\delta_t\phi^{n+1}dK - 2\int_{\partial K}\widehat{\boldsymbol{w}}^n\cdot\boldsymbol{\nu}\delta_t\phi^{n+1}ds. \tag{4.6}$$

From (4.2g), we have

$$\int_K \boldsymbol{w}^n\cdot\boldsymbol{\theta}_4 dK = -\int_K \phi^n\nabla\cdot\boldsymbol{\theta}_4 dK + \int_{\partial K}\widehat{\phi}^n\boldsymbol{\theta}_4\cdot\boldsymbol{\nu}ds. \tag{4.7}$$

Choosing the test function $\boldsymbol{\theta}_4 = -2\delta_t\boldsymbol{w}^{n+1}$ and $\boldsymbol{\theta}_4 = \frac{1}{\Delta t}\boldsymbol{q}_1^{n+1}$ in (4.7), we obtain

$$-2\int_K \boldsymbol{w}^n\cdot\delta_t\boldsymbol{w}^{n+1}dK = 2\int_K \phi^n\nabla\cdot\delta_t\boldsymbol{w}^{n+1}dK - 2\int_{\partial K}\widehat{\phi}^n\delta_t\boldsymbol{w}^{n+1}\cdot\boldsymbol{\nu}ds, \tag{4.8a}$$

$$\frac{1}{\Delta t}\int_K \boldsymbol{w}^n\cdot\boldsymbol{q}_1^{n+1}dK = -\frac{1}{\Delta t}\int_K \phi^n\nabla\cdot\boldsymbol{q}_1^{n+1}dK + \frac{1}{\Delta t}\int_{\partial K}\widehat{\phi}^n\boldsymbol{q}_1^{n+1}\cdot\boldsymbol{\nu}ds. \tag{4.8b}$$

Combining (4.4), (4.6), and (4.8), we get

(4.9)
$$\begin{aligned}
&\int_K (q^{n+1}\delta_t q^{n+1} - 2\boldsymbol{w}^n\cdot\delta_t\boldsymbol{w}^{n+1} + ((\phi^{n+1})^3 + (1-\epsilon)\phi^{n+1})\delta_t\phi^{n+1})dK \\
&+ \int_K M(\phi^n)\boldsymbol{s}^{n+1}\cdot\boldsymbol{s}^{n+1}dK \\
=&-\int_K \nabla\cdot((r^{n+1}+2q^n+q_2^{n+1})\boldsymbol{p}^{n+1})dK + \int_{\partial K}(\widehat{\boldsymbol{p}}^{n+1}\cdot\boldsymbol{\nu}(r^{n+1}+2q^n+q_2^{n+1}) \\
&+ (\widehat{r}^{n+1}+2\widehat{q}^n+\widehat{q}_2^{n+1})\boldsymbol{p}^{n+1}\cdot\boldsymbol{\nu})ds + \int_K \nabla\cdot(\delta_t\phi^{n+1}\boldsymbol{q}_1^{n+1})dK - \int_{\partial K}(\widehat{\delta_t\phi^{n+1}}\boldsymbol{q}_1^{n+1}\cdot\boldsymbol{\nu} \\
&+ \widehat{\boldsymbol{q}}_1^{n+1}\cdot\boldsymbol{\nu}\delta_t\phi^{n+1})ds - \frac{1}{\Delta t}\int_K \nabla\cdot(q^{n+1}\boldsymbol{w}^{n+1})dK \\
&+ \frac{1}{\Delta t}\int_{\partial K}(\widehat{q}^{n+1}\boldsymbol{w}^{n+1}\cdot\boldsymbol{\nu} + \widehat{\boldsymbol{w}}^{n+1}\cdot\boldsymbol{\nu}q^{n+1})ds \\
&+ \frac{1}{\Delta t}\int_K (q^{n+1}\nabla\cdot\boldsymbol{w}^n + \boldsymbol{w}^{n+1}\cdot\nabla q^n)dK - \frac{1}{\Delta t}\int_{\partial K}(\widehat{q}^{n+1}\boldsymbol{w}^n\cdot\boldsymbol{\nu} + \widehat{\boldsymbol{w}}^{n+1}\cdot\boldsymbol{\nu}q^n)ds \\
&- \frac{2}{\Delta t}\int_K \nabla\cdot(\phi^n\boldsymbol{w}^n)dK + \frac{2}{\Delta t}\int_{\partial K}(\widehat{\boldsymbol{w}}^n\cdot\boldsymbol{\nu}\phi^n + \widehat{\phi}^n\boldsymbol{w}^n\cdot\boldsymbol{\nu})ds \\
&+ \frac{2}{\Delta t}\int_K (\boldsymbol{w}^n\cdot\nabla\phi^{n+1} + \phi^n\nabla\cdot\boldsymbol{w}^{n+1})dK - \frac{2}{\Delta t}\int_{\partial K}(\widehat{\boldsymbol{w}}^n\cdot\boldsymbol{\nu}\phi^{n+1} + \widehat{\phi}^n\boldsymbol{w}^{n+1}\cdot\boldsymbol{\nu})ds.
\end{aligned}$$

For (4.2f), we choose the test function as $\varphi_3 = q^n$ and obtain

$$\int_K q^{n+1}q^n dK = -\int_K \boldsymbol{w}^{n+1}\cdot\nabla q^n dK + \int_{\partial K}\widehat{\boldsymbol{w}}^{n+1}\cdot\boldsymbol{\nu}q^n ds, \tag{4.10}$$

while for (4.5), we choose the test function as $\varphi_3 = q^{n+1}$ and obtain

$$\int_K q^n q^{n+1}dK = -\int_K \boldsymbol{w}^n\cdot\nabla q^{n+1}dK + \int_{\partial K}\widehat{\boldsymbol{w}}^n\cdot\boldsymbol{\nu}q^{n+1}ds. \tag{4.11}$$

By substituting (4.10) and (4.11), we have

$$\begin{aligned}
&\int_K (q^{n+1}\nabla\cdot\boldsymbol{w}^n + \boldsymbol{w}^{n+1}\cdot\nabla q^n)dK - \int_{\partial K}(\widehat{q}^{n+1}\boldsymbol{w}^n\cdot\boldsymbol{\nu} + \widehat{\boldsymbol{w}}^{n+1}\cdot\boldsymbol{\nu}q^n)ds \qquad (4.12)\\
&\overset{(4.10)}{=} \int_K (q^{n+1}\nabla\cdot\boldsymbol{w}^n - q^{n+1}q^n)dK - \int_{\partial K}\widehat{q}^{n+1}\boldsymbol{w}^n\cdot\boldsymbol{\nu}ds \\
&\overset{(4.11)}{=} \int_K \nabla\cdot(q^{n+1}\boldsymbol{w}^n) - \int_{\partial K}(\widehat{\boldsymbol{w}}^n\cdot\boldsymbol{\nu}q^{n+1} + \widehat{q}^{n+1}\boldsymbol{w}^n\cdot\boldsymbol{\nu})ds.
\end{aligned}$$

By the same technique as above, we have

$$\begin{aligned}
&\int_K (\boldsymbol{w}^n\cdot\nabla\phi^{n+1} + \phi^n\nabla\cdot\boldsymbol{w}^{n+1})dK - \int_{\partial K}(\widehat{\boldsymbol{w}}^n\cdot\boldsymbol{\nu}\phi^{n+1} + \widehat{\phi}^n\boldsymbol{w}^{n+1}\cdot\boldsymbol{\nu})ds \qquad (4.13)\\
&= \int_K \nabla\cdot(\phi^{n+1}\boldsymbol{w}^n)dK - \int_{\partial K}(\widehat{\phi}^{n+1}\boldsymbol{w}^n\cdot\boldsymbol{\nu} + \widehat{\boldsymbol{w}}^n\cdot\boldsymbol{\nu}\phi^{n+1})ds.
\end{aligned}$$

Finally, summing up (4.9) over K, using (4.12)–(4.13), and noticing the fluxes in (4.3) are from the opposite sides of ∂K as well as the boundary conditions, we get

$$\int_\Omega (q^{n+1}\delta_t q^{n+1} - 2\boldsymbol{w}^n \cdot \delta_t \boldsymbol{w}^{n+1} + ((\phi^{n+1})^3 + (1-\epsilon)\phi^{n+1})\delta_t \phi^{n+1}) d\boldsymbol{x} + \int_\Omega M(\phi^n)\boldsymbol{s}^{n+1} \cdot \boldsymbol{s}^{n+1} d\boldsymbol{x} = 0.$$

Then

$$\int_\Omega (q^{n+1}\delta_t q^{n+1} - 2\boldsymbol{w}^n \cdot \delta_t \boldsymbol{w}^{n+1}) d\boldsymbol{x} + \int_\Omega M(\phi^n)\boldsymbol{s}^{n+1} \cdot \boldsymbol{s}^{n+1} d\boldsymbol{x}$$
$$+ \frac{1}{\Delta t}\int_\Omega \left(\frac{1}{4}(\phi^{n+1})^4 + \frac{1-\epsilon}{2}(\phi^{n+1})^2\right) d\boldsymbol{x} - \frac{1}{\Delta t}\int_\Omega \left(\frac{1}{4}(\phi^{n})^4 + \frac{1-\epsilon}{2}(\phi^{n})^2\right) d\boldsymbol{x}$$
$$+ \frac{1}{4\Delta t}\int_\Omega \left((2 - 2\epsilon + 2(\phi^{n+1})^2 + (\phi^n + \phi^{n+1})^2)(\phi^{n+1} - \phi^n)^2\right) d\boldsymbol{x} = 0;$$

therefore we obtain the discrete energy stability

$$\frac{1}{\Delta t}\left[\int_\Omega \left(\frac{1}{2}(q^{n+1})^2 - \boldsymbol{w}^{n+1}\cdot\boldsymbol{w}^{n+1} + \frac{1}{4}(\phi^{n+1})^4 + \frac{1-\epsilon}{2}(\phi^{n+1})^2\right) d\boldsymbol{x}\right]$$
$$+ \int_\Omega M(\phi^n)\boldsymbol{s}^{n+1}\cdot\boldsymbol{s}^{n+1} d\boldsymbol{x}$$
$$\le \frac{1}{\Delta t}\left[\int_\Omega \left(\frac{1}{2}(q^{n})^2 - \boldsymbol{w}^{n}\cdot\boldsymbol{w}^{n} + \frac{1}{4}(\phi^{n})^4 + \frac{1-\epsilon}{2}(\phi^{n})^2\right) d\boldsymbol{x}\right]. \qquad \square$$

Remark 4.2. The unconditional energy stability is proved. But as for the solvability of the convex splitting scheme, the proof is not easy in the LDG framework. Even though the auxiliary variables in the LDG method give the easy treatment for nonlinear and high order derivative terms, the theoretical analysis of solvability for the LDG is more troublesome because of the auxiliary variables. We will leave it to our future work.

Remark 4.3. Equations (4.2) at the implicit time level are nonlinear; we will employ a nonlinear full approximation storage (FAS) multigrid method [2] to solve the equations.

4.2. Second-order convex splitting scheme. Hu et al. introduced a second order convex splitting scheme for PFC equation in [11], which is given as

$$\frac{\phi^{n+1}-\phi^n}{\Delta t} = \nabla\cdot\left(M\left(\frac{3}{2}\phi^n - \frac{1}{2}\phi^{n-1}\right)\nabla\mu^{n+1}\right), \tag{4.14}$$

$$\mu^{n+1} = \frac{1}{4}(\phi^{n+1}+\phi^n)((\phi^{n+1})^2 + (\phi^n)^2) + \frac{1-\epsilon}{2}(\phi^{n+1}+\phi^n) + 3\Delta\phi^n - \Delta\phi^{n-1} + \frac{1}{2}(\Delta^2\phi^{n+1} + \Delta^2\phi^n), \tag{4.15}$$

where $\phi^{-1} := \phi^0$. The LDG method to solve the second order scheme (4.14) becomes the following: Find ϕ^{n+1}, q_2^{n+1}, q^{n+1}, $r^{n+1} \in V_h$ and $\boldsymbol{p}^{n+1}$, $\boldsymbol{s}^{n+1}$, $\boldsymbol{q}_1^{n+1}$, $\boldsymbol{w}^{n+1} \in \Sigma_h^d$ such that, for all test functions φ_1, φ_2, φ_3, $\varphi_4 \in V_h$ and $\boldsymbol{\theta}_1$, $\boldsymbol{\theta}_2$, $\boldsymbol{\theta}_3$, $\boldsymbol{\theta}_4 \in \Sigma_h^d$, we have

$$\int_K \frac{\phi^{n+1}-\phi^n}{\Delta t}\varphi_1 dK = -\int_K \boldsymbol{p}^{n+1}\cdot\nabla\varphi_1 dK + \int_{\partial K}\widehat{\boldsymbol{p}}^{n+1}\cdot\boldsymbol{\nu}\varphi_1 ds, \tag{4.16a}$$

$$\int_K \boldsymbol{p}^{n+1}\cdot\boldsymbol{\theta}_1 dK = \int_K M\left(\frac{3}{2}\phi^n - \frac{1}{2}\phi^{n-1}\right)\boldsymbol{s}^{n+1}\cdot\boldsymbol{\theta}_1 dK, \tag{4.16b}$$

$$\int_K \boldsymbol{s}^{n+1}\cdot\boldsymbol{\theta}_2 dK = -\int_K \left(r^{n+1}+3q^n-q^{n-1}+\frac{1}{2}q_2^{n+1}+\frac{1}{2}q_2^n\right)\nabla\cdot\boldsymbol{\theta}_2 dK + \int_{\partial K}\left(\widehat{r}^{n+1}+3\widehat{q}^n-\widehat{q}^{n-1}+\frac{1}{2}\widehat{q}_2^{n+1}+\frac{1}{2}\widehat{q}_2^n\right)\boldsymbol{\theta}_2\cdot\boldsymbol{\nu} ds, \tag{4.16c}$$

$$\int_K q_2^{n+1}\varphi_2 dK = -\int_K \boldsymbol{q}_1^{n+1}\cdot\nabla\varphi_2 dK + \int_{\partial K}\widehat{\boldsymbol{q}}_1^{n+1}\cdot\boldsymbol{\nu}\varphi_2 ds, \tag{4.16d}$$

$$\int_K \boldsymbol{q}_1^{n+1}\cdot\boldsymbol{\theta}_3 dK = -\int_K q^{n+1}\nabla\cdot\boldsymbol{\theta}_3 dK + \int_{\partial K}\widehat{q}^{n+1}\boldsymbol{\theta}_3\cdot\boldsymbol{\nu} ds, \tag{4.16e}$$

$$\int_K q^{n+1}\varphi_3 dK = -\int_K \boldsymbol{w}^{n+1}\cdot\nabla\varphi_3 dK + \int_{\partial K}\widehat{\boldsymbol{w}}^{n+1}\cdot\boldsymbol{\nu}\varphi_3 ds, \tag{4.16f}$$

$$\int_K \boldsymbol{w}^{n+1}\cdot\boldsymbol{\theta}_4 dK = -\int_K \phi^{n+1}\nabla\cdot\boldsymbol{\theta}_4 dK + \int_{\partial K}\widehat{\phi}^{n+1}\boldsymbol{\theta}_4\cdot\boldsymbol{\nu} ds, \tag{4.16g}$$

$$\int_K r^{n+1}\varphi_4 dK = \int_K \left(\frac{1}{4}(\phi^{n+1}+\phi^n)((\phi^{n+1})^2+(\phi^n)^2) + \frac{1-\epsilon}{2}(\phi^{n+1}+\phi^n)\right)\varphi_4 dK. \tag{4.16h}$$

Next, we will prove the unconditional discrete energy stability for the second order fully discrete LDG scheme (4.16).

PROPOSITION 4.4 (energy stability for the fully discrete LDG scheme with second order convex splitting scheme). *The solution to the LDG scheme* (4.16) *with the flux* (4.3) *satisfies the discrete energy dissipative*

$$E_h(\phi^{n+1},\boldsymbol{w}^{n+1},q^{n+1})-E_h(\phi^0,\boldsymbol{w}^0,q^0)\le 0,$$

where $E_h(\phi,\boldsymbol{w},q)=\int_\Omega\left(\frac{1}{4}\phi^4+\frac{1-\epsilon}{2}\phi^2-\boldsymbol{w}\cdot\boldsymbol{w}+\frac{1}{2}q^2\right)d\boldsymbol{x}$.

Proof. For (4.16f), choosing the test function $\varphi_3=-3\delta_t\phi^{n+1}$ at time level t^n and $\varphi_3=\delta_t\phi^{n+1}$ at time level t^{n-1} show that

$$-3\int_K q^n\delta_t\phi^{n+1}dK = 3\int_K \boldsymbol{w}^n\cdot\nabla\delta_t\phi^{n+1}dK - 3\int_{\partial K}\widehat{\boldsymbol{w}}^n\cdot\boldsymbol{\nu}\delta_t\phi^{n+1}ds, \tag{4.17}$$

$$\int_K q^{n-1}\delta_t\phi^{n+1}dK = -\int_K \boldsymbol{w}^{n-1}\cdot\nabla\delta_t\phi^{n+1}dK + \int_{\partial K}\widehat{\boldsymbol{w}}^{n-1}\cdot\boldsymbol{\nu}\delta_t\phi^{n+1}ds. \tag{4.18}$$

For (4.16d), (4.16e), taking the sum between time level t^{n+1} and t^n, and choosing test functions $\varphi_2=-\frac{1}{2}\delta_t\phi^{n+1}$, $\boldsymbol{\theta}_3=\frac{1}{2}\delta_t\boldsymbol{w}^{n+1}$, respectively, we have

$$-\frac{1}{2}\int_K(q_2^{n+1}+q_2^n)\delta_t\phi^{n+1}dK = \frac{1}{2}\int_K(\boldsymbol{q}_1^{n+1}+\boldsymbol{q}_1^n)\cdot\nabla\delta_t\phi^{n+1}dK - \frac{1}{2}\int_{\partial K}(\widehat{\boldsymbol{q}}_1^{n+1}+\widehat{\boldsymbol{q}}_1^n)\cdot\boldsymbol{\nu}\delta_t\phi^{n+1}ds, \tag{4.19}$$

$$\frac{1}{2}\int_K(\boldsymbol{q}_1^{n+1}+\boldsymbol{q}_1^n)\cdot\delta_t\boldsymbol{w}^{n+1}dK = -\frac{1}{2}\int_K(q^{n+1}+q^n)\nabla\cdot\delta_t\boldsymbol{w}^{n+1}dK + \frac{1}{2}\int_{\partial K}(\widehat{q}^{n+1}+\widehat{q}^n)\delta_t\boldsymbol{w}^{n+1}\cdot\boldsymbol{\nu}ds. \tag{4.20}$$

For (4.16f), (4.16g), taking the difference between time level t^{n+1} and t^n, and choosing test functions

$$\varphi_3=\frac{1}{2\Delta t}(q^{n+1}+q^n),\qquad \boldsymbol{\theta}_4=\frac{1}{\Delta t}\left(-\frac{1}{2}\boldsymbol{q}_1^{n+1}-\frac{1}{2}\boldsymbol{q}_1^n-3\boldsymbol{w}^n+\boldsymbol{w}^{n-1}\right),$$

respectively, we have

$$\begin{aligned}
&\frac{1}{2}\int_K(\delta_t q^{n+1})(q^{n+1}+q^n)dK\\
=&-\frac{1}{2}\int_K(\delta_t \boldsymbol{w}^{n+1})\cdot\nabla(q^{n+1}+q^n)dK\\
&+\frac{1}{2}\int_{\partial K}(\delta_t \widehat{\boldsymbol{w}}^{n+1})\cdot\boldsymbol{\nu}(q^{n+1}+q^n)ds,
\end{aligned}\tag{4.21}$$

$$\begin{aligned}
&\int_K(\delta_t \boldsymbol{w}^{n+1})\cdot\left(\boldsymbol{w}^{n-1}-3\boldsymbol{w}^n-\frac{1}{2}\boldsymbol{q}_1^{n+1}-\frac{1}{2}\boldsymbol{q}_1^n\right)dK\\
=&-\int_K(\delta_t\phi^{n+1})\nabla\cdot\left(\boldsymbol{w}^{n-1}-3\boldsymbol{w}^n-\frac{1}{2}\boldsymbol{q}_1^{n+1}-\frac{1}{2}\boldsymbol{q}_1^n\right)dK\\
&+\int_{\partial K}(\delta_t\widehat{\phi}^{n+1})\left(\boldsymbol{w}^{n-1}-3\boldsymbol{w}^n-\frac{1}{2}\boldsymbol{q}_1^{n+1}-\frac{1}{2}\boldsymbol{q}_1^n\right)\cdot\boldsymbol{\nu}ds.
\end{aligned}\tag{4.22}$$

For other equations in scheme (4.16), we choose the test functions as

$$\varphi_1=r^{n+1}+3q^n-q^{n-1}+\frac{1}{2}q_2^{n+1}+\frac{1}{2}q_2^n,\quad \boldsymbol{\theta}_1=-\boldsymbol{s}^{n+1},\quad \boldsymbol{\theta}_2=\boldsymbol{p}^{n+1},\quad \varphi_4=-\delta_t\phi^{n+1},$$

to get

$$\begin{aligned}
&\int_K\delta_t\phi^{n+1}\left(r^{n+1}+3q^n-q^{n-1}+\frac{1}{2}q_2^{n+1}+\frac{1}{2}q_2^n\right)dK\\
=&-\int_K\boldsymbol{p}^{n+1}\cdot\nabla\left(r^{n+1}+3q^n-q^{n-1}+\frac{1}{2}q_2^{n+1}+\frac{1}{2}q_2^n\right)dK\\
&+\int_{\partial K}\widehat{\boldsymbol{p}}^{n+1}\cdot\boldsymbol{\nu}\left(r^{n+1}+3q^n-q^{n-1}+\frac{1}{2}q_2^{n+1}+\frac{1}{2}q_2^n\right)ds,
\end{aligned}\tag{4.23}$$

$$-\int_K\boldsymbol{p}^{n+1}\cdot\boldsymbol{s}^{n+1}dK=-\int_K M\left(\frac{3}{2}\phi^n-\frac{1}{2}\phi^{n-1}\right)\boldsymbol{s}^{n+1}\cdot\boldsymbol{s}^{n+1}dK,\tag{4.24}$$

$$\begin{aligned}
\int_K\boldsymbol{s}^{n+1}\cdot\boldsymbol{p}^{n+1}dK=&-\int_K\left(r^{n+1}+3q^n-q^{n-1}+\frac{1}{2}q_2^{n+1}+\frac{1}{2}q_2^n\right)\nabla\cdot\boldsymbol{p}^{n+1}dK\\
&+\int_{\partial K}\left(\widehat{r}^{n+1}+3\widehat{q}^n-\widehat{q}^{n-1}+\frac{1}{2}\widehat{q}_2^{n+1}+\frac{1}{2}\widehat{q}_2^n\right)\boldsymbol{p}^{n+1}\cdot\boldsymbol{\nu}ds,
\end{aligned}\tag{4.25}$$

$$\begin{aligned}
-\int_K r^{n+1}\delta_t\phi^{n+1}dK=&-\int_K\left(\frac{1}{4}(\phi^{n+1}+\phi^n)((\phi^{n+1})^2+(\phi^n)^2)\right.\\
&\left.+\frac{1-\epsilon}{2}(\phi^{n+1}+\phi^n)\right)\delta_t\phi^{n+1}dK.
\end{aligned}\tag{4.26}$$

Let (4.17)+(4.18)+$\cdots$+(4.25)+(4.26), with the help of the alternating numerical fluxes (4.3), and after a careful calculation, we obtain

$$\begin{aligned}
&\frac{1}{2\Delta t}\int_\Omega((q^{n+1})^2-(q^n)^2)d\boldsymbol{x}+\frac{1}{\Delta t}\int_\Omega\left(\frac{1}{4}(\phi^{n+1})^4+\frac{1-\epsilon}{2}(\phi^{n+1})^2\right)d\boldsymbol{x}\\
&-\frac{1}{\Delta t}\int_\Omega\left(\frac{1}{4}(\phi^n)^4+\frac{1-\epsilon}{2}(\phi^n)^2\right)d\boldsymbol{x}+\frac{1}{\Delta t}\int_\Omega(-3\boldsymbol{w}^n+\boldsymbol{w}^{n-1})\cdot(\boldsymbol{w}^{n+1}-\boldsymbol{w}^n)d\boldsymbol{x}\\
&+\int_\Omega M\left(\frac{3}{2}\phi^n-\frac{1}{2}\phi^{n-1}\right)\boldsymbol{s}^{n+1}\cdot\boldsymbol{s}^{n+1}d\boldsymbol{x}=0.
\end{aligned}$$

Notice that

$$\begin{aligned}&(-3\boldsymbol{w}^n+\boldsymbol{w}^{n-1})\cdot(\boldsymbol{w}^{n+1}-\boldsymbol{w}^n)\\&=-\boldsymbol{w}^{n+1}\cdot\boldsymbol{w}^{n+1}+\boldsymbol{w}^n\cdot\boldsymbol{w}^n+\frac{1}{2}(\boldsymbol{w}^{n+1}-2\boldsymbol{w}^n+\boldsymbol{w}^{n-1})\cdot(\boldsymbol{w}^{n+1}-2\boldsymbol{w}^n+\boldsymbol{w}^{n-1})\\&\quad+\frac{1}{2}(\boldsymbol{w}^{n+1}-\boldsymbol{w}^n)\cdot(\boldsymbol{w}^{n+1}-\boldsymbol{w}^n)-\frac{1}{2}(\boldsymbol{w}^n-\boldsymbol{w}^{n-1})\cdot(\boldsymbol{w}^n-\boldsymbol{w}^{n-1}).\end{aligned}$$

Therefore we have

(4.27)

$$\begin{aligned}&E_h(\phi^{n+1},\boldsymbol{w}^{n+1},q^{n+1})-E_h(\phi^n,\boldsymbol{w}^n,q^n)\\&\le-\frac{1}{2}\int_\Omega(\boldsymbol{w}^{n+1}-\boldsymbol{w}^n)\cdot(\boldsymbol{w}^{n+1}-\boldsymbol{w}^n)d\boldsymbol{x}+\frac{1}{2}\int_\Omega(\boldsymbol{w}^n-\boldsymbol{w}^{n-1})\cdot(\boldsymbol{w}^n-\boldsymbol{w}^{n-1})d\boldsymbol{x}.\end{aligned}$$

Summing (4.27), with the condition $\phi^0=\phi^{-1}$, we have

$$E_h(\phi^{n+1},\boldsymbol{w}^{n+1},q^{n+1})-E_h(\phi^0,\boldsymbol{w}^0,q^0)\le 0, \tag{4.28}$$

which is the energy stability result. ∎

Remark 4.5. The energy stability for the semidiscrete LDG scheme (3.2), fully discrete convex splitting scheme (4.2), and second order fully discrete LDG scheme (4.16) for variables ϕ, $\boldsymbol{w}$, and q is proved in Propositions 3.1, 4.1, and 4.4, respectively. The numerical solutions with LDG spatial discretization are discontinuous piecewise polynomials, which leads to that the numerical solutions for ϕ, $\boldsymbol{w}$, and q are in $L^2(\Omega)$ space but not on $H^2(\Omega)$ space. Therefore, H^2-stability for the numerical solution ϕ will not be proved.

Remark 4.6. The convergence analysis for the convex splitting scheme (4.2) and the second scheme (4.16) in the LDG framework on solving high order time-dependent equations are much more elusive. The main technical difficulty is the lack of control on the auxiliary variables in the LDG method which are approximations to the derivatives of the solution, and the lack of control on the interface boundary terms. Since the PFC equation is a fully nonlinear high order time-dependent equation, the convergence analysis for the convex splitting scheme is very difficult and we will leave this topic as our future work.

The first order and second order convex splitting schemes are stable regardless of time step. However, the schemes are only first order or second order accurate in time. To improve the temporal accuracy, the semi-implicit spectral deferred correction (SDC) method and a high order semi-implicit Runge–Kutta method combining with the first order convex splitting scheme will be employed in the next subsections for the PFC equation with constant and degenerate mobility, respectively.

4.3. The semi-implicit SDC method. For the PFC equation with constant mobility, i.e., $M(\phi)$ is constant, we can apply the semi-implicit SDC method based on the convex splitting scheme (4.1) to achieve high order temporal accuracy. An advantage of this method is that it is a one-step method and can be constructed easily and systematically for any order of accuracy. For convenience, the convex splitting scheme (4.1) can be rewritten as

$$\phi^{n+1}=\phi^n+\Delta t(F_S(\phi^{n+1})+F_N(\phi^n)), \tag{4.29}$$

where $F_S(\phi)$ represents the implicit part and $F_N(\phi)$ represents the explicit part of the convex splitting scheme, which means

$$F_S(\phi) = \Delta(\phi^3 + (1-\epsilon)\phi + \Delta^2\phi), \qquad F_N(\phi) = 2\Delta^2\phi. \tag{4.30}$$

Then the semi-implicit SDC method can be applied iteratively. For a detailed description of the SDC method as well as their implementation and applications, we refer the readers to [7, 12, 17, 18].

4.4. The semi-implicit Runge–Kutta method. For the PFC equation with degenerate mobility, i.e., $M(\phi)$ is not constant, as we know, the stiff and nonstiff components cannot be well separated as a form of (4.29). In this case, the semi-implicit SDC method will not be efficient anymore. Based on the work in [1], the main idea of the semi-implicit Runge–Kutta method is to apply two different Runge–Kutta methods. Consider the ODE system

$$\begin{cases} u_t = F(t, u(t), v(t)), \quad t \in [0, T], \\ u(0) = u_0, \quad v(0) = u_0, \end{cases} \tag{4.31}$$

where the function $F : \mathbb{R} \times \mathbb{R}^m \times \mathbb{R}^m \to \mathbb{R}^m$ is sufficiently differentiable and the dependence on the second argument of F is nonstiff, while the dependence on the third argument is stiff.

To derive the high order semi-implicit Runge–Kutta method, we first rewrite the system (4.31) as

$$\begin{cases} u_t = F(t, u(t), v(t)), \\ v_t = F(t, u(t), v(t)), \end{cases} \tag{4.32}$$

with initial conditions $u(0) = u_0$, $v(0) = u_0$. Then the first variable u is treated explicitly and the second one v is treated implicitly. The semi-implicit Runge–Kutta method is a multistage method. Starting from u^n, we give the algorithm to calculate u^{n+1} in the following:

$$\begin{aligned} &U_1 = V_1 = u^n, \\ &U_i = u^n + \Delta t \sum_{j=1}^{i-1} \hat{a}_{ij} k_j, \quad 2 \le i \le s, \\ &V_i = u^n + \Delta t \sum_{j=1}^{i-1} a_{ij} l_j, \quad 2 \le i \le s, \\ &l_i = F(t^n + c_i \Delta t, U_i, V_i + \Delta t a_{ii} l_i), \quad 1 \le i \le s, \\ &k_i = F(t^n + \hat{c}_i \Delta t, U_i, V_i + \Delta t a_{ii} l_i), \quad 1 \le i \le s. \end{aligned} \tag{4.33}$$

Finally we have

$$u^{n+1} = u^n + \Delta t \sum_{i=1}^{s} b_i k_i. \tag{4.34}$$

The Butcher coefficients a_{ij}, $\hat{a}_{i,j}$, c_j, $\hat{c}_j$, and b_j are constrained by order of accuracy and stability considerations. For a detailed description of the methods as well as their implementation and applications, we refer the readers to [1].

After the LDG spatial discretization for the PFC equation, we apply the semi-implicit scheme (4.33)–(4.34) by writing the system of ODE in the form of (4.31) with the component u treated explicitly, the component v treated implicitly and

$$F(t,u,v) = \nabla \cdot (M(u)\nabla(v^3 + (1-\epsilon)v + 2\Delta u + \Delta^2 v)), \tag{4.35}$$

which is based on the convex splitting scheme (4.1).

5. Numerical tests. In this section, we present some numerical experiments for the PFC model. Specifically, we adopt the LDG spatial discretization coupled with the convex splitting time marching methods. To achieve high order temporal accuracy, we also use the semi-implicit SDC method and the semi-implicit Runge–Kutta method described above. The resulting nonlinear algebraic equations at each step are solved by the FAS multigrid solver. All the computations are performed in double precision.

Example 5.1 (accuracy test for PFC equation with constant mobility). To demonstrate the superiority of the multigrid solver, we present the convergence rates of the method. For the tests we take the exact solution of

$$\phi(x,y,t) = e^{-2t}\sin(x)\sin(y), \tag{5.1}$$

with the source term $f(x,y,t)$, where $f(x,y,t)$ is a given function to make (5.1) be the exact solution of the PFC equation. The initial condition is

$$\phi(x,y,0) = \sin(x)\sin(y), \tag{5.2}$$

and the domain is $[0,2\pi]\times[0,2\pi]$ with periodic boundary conditions. The parameter ϵ in the PFC model is 0.5.

We first consider the convex splitting scheme (4.1), which is first order accurate in time, so we just consider $\mathcal{P}^0$ approximation. The L^2 and L^∞ errors, and the numerical order of accuracy at time $T = 1.0$ with different time steps is presented in Table 5.1. Here, we perform numerical simulation with different time steps for convex splitting scheme to demonstrate that the numerical experiments go well with the theoretical result of the unconditional energy stability. Table 5.2 shows the proposed second order scheme (4.14) is second order accurate in time.

To show that the proposed space and time discretization methods are high order accurate in both space and time, we choose $\mathcal{P}^k (k \geq 1)$ approximation for spatial discretization and third order SDC time marching method. Table 5.3 shows the L^2 and L^∞ errors and numerical orders of accuracy at time $T = 0.5$. We can see that the method with $\mathcal{P}^k$ approximation gives a $(k+1)$th order of accuracy.

To illustrate the superiority of the multigrid solver, we fix the temporal step size as $\Delta t = 1.0 \times 10^{-3}$ and present the convergence rates of the multigrid solver at the $10th$ time step, and the results are shown in Figure 5.1. From Figure 5.1, we can see the optimal convergence rate of the multigrid solver for $\mathcal{P}^1$ and $\mathcal{P}^2$ approximation, which suggests that the multigrid solver is very efficient for solving the resulting algebraic system at each time step.

Example 5.2 (accuracy test for PFC equation with degenerate mobility). Consider the PFC equation (2.4) with degenerate mobility, i.e., $M(\phi) = 1 - \phi^2$ on the domain $[0,2\pi]\times[0,2\pi]$ with periodic boundary conditions. For the tests we take the exact solution of

$$\phi(x,y,t) = e^{-2t}\sin(x)\sin(y), \tag{5.3}$$

TABLE 5.1

Accuracy test for PFC equation with constant mobility with first order convex splitting scheme at $T = 1.0$.

	$\Delta t = 0.1\Delta x$				$\Delta t = 1.0\Delta x$			
N	L^2 error	Order	L^∞ error	Order	L^2 error	Order	L^∞ error	Order
16	6.75E-02	–	1.39E-01	–	2.52E-01	–	4.95E-01	–
32	3.34E-02	1.01	6.82E-02	1.03	1.83E-01	0.46	3.66E-01	0.43
64	1.65E-02	1.01	3.38E-02	1.01	1.16E-01	0.65	2.33E-01	0.65
128	8.23E-03	1.00	1.68E-02	1.00	6.78E-02	0.78	1.35E-01	0.78
	$\Delta t = 5.0\Delta x$				$\Delta t = 10.0\Delta x$			
N	L^2 error	Order	L^∞ error	Order	L^2 error	Order	L^∞ error	Order
16	3.53E-01	–	6.93E-01	–	3.53E-01	–	6.93E-01	–
32	3.42E-01	0.05	6.79E-01	0.03	3.54E-01	–	7.06E-01	–
64	2.79E-01	0.29	5.57E-01	0.29	3.42E-01	0.05	6.81E-01	0.05
128	2.05E-01	0.44	4.11E-01	0.44	2.79E-01	0.29	5.57E-01	0.29

TABLE 5.2

Accuracy test for PFC equation with constant mobility with second order convex splitting scheme at $T = 0.5$. $\Delta t = 0.1\Delta x$.

	N	L^2 error	Order	L^∞ error	Order
$\mathcal{P}^1$	8	1.41E-02	–	6.45E-02	–
	16	3.45E-03	2.02	1.65E-02	1.96
	32	8.63E-04	2.00	4.15E-03	1.99
	64	2.15E-04	2.00	1.04E-03	1.98

TABLE 5.3

Accuracy test for PFC equation with constant mobility with third order SDC method at $T = 0.5$. $\Delta t = 0.1\Delta x$.

	N	L^2 error	Order	L^∞ error	Order
$\mathcal{P}^1$	8	1.38E-02	–	6.27E-02	–
	16	3.39E-03	2.02	1.58E-02	1.98
	32	8.48E-04	2.00	3.92E-03	2.01
	64	2.12E-04	2.00	9.75E-04	2.00
$\mathcal{P}^2$	8	2.21E-03	–	1.08E-02	–
	16	2.32E-04	3.25	1.28E-03	3.08
	32	2.76E-05	3.06	1.57E-04	3.03
	64	3.48E-06	3.00	1.99E-05	2.98

TABLE 5.4

Accuracy test for PFC equation with degenerate mobility with first order convex splitting scheme at $T = 1.0$.

	$\Delta t = 0.1\Delta x$				$\Delta t = 1.0\Delta x$			
N	L^2 error	Order	L^∞ error	Order	L^2 error	Order	L^∞ error	Order
16	6.30E-02	–	1.32E-01	–	2.22E-01	–	4.37E-01	–
32	3.12E-02	1.01	6.46E-02	1.03	1.63E-01	0.44	3.26E-01	0.42
64	1.54E-02	1.01	3.21E-02	1.01	1.05E-01	0.63	2.11E-01	0.63
128	7.70E-03	1.00	1.59E-02	1.00	6.20E-02	0.77	1.24E-01	0.77
	$\Delta t = 5.0\Delta x$				$\Delta t = 10.0\Delta x$			
N	L^2 error	Order	L^∞ error	Order	L^2 error	Order	L^∞ error	Order
16	3.08E-01	–	6.03E-01	–	3.08E-01	–	6.03E-01	–
32	2.98E-01	0.05	5.93E-01	0.02	3.07E-01	–	6.09E-01	–
64	2.44E-01	0.29	4.87E-01	0.28	2.98E-01	0.05	5.93E-01	0.04
128	1.82E-01	0.42	3.63E-01	0.42	2.44E-01	0.29	4.86E-01	0.29

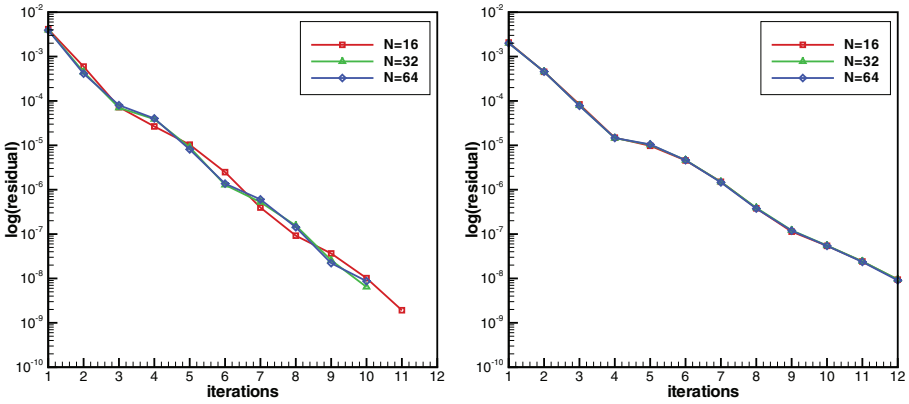

(a) $\mathcal{P}^1$ approximation (b) $\mathcal{P}^2$ approximation

FIG. 5.1. *Convergence rates of multigrid solver with* $\mathcal{P}^1$ *and* $\mathcal{P}^2$ *approximation for Example* 5.1.

TABLE 5.5

Accuracy test for PFC equation with degenerate mobility with second order convex splitting scheme at $T = 0.5$. $\Delta t = 0.1\Delta x$.

	N	L^2 error	Order	L^∞ error	Order
$\mathcal{P}^1$	8	1.37E-02	–	6.07E-02	–
	16	3.41E-03	2.00	1.59E-02	1.93
	32	8.54E-04	2.00	4.04E-03	1.98
	64	2.13E-04	2.00	1.02E-03	1.98

with the source term $f(x, y, t)$, where $f(x, y, t)$ is a given function to make (5.3) be the exact solution of the PFC equation. Choose the parameter $\epsilon = 0.5$. The L^2 and L^∞ errors and the numerical order of accuracy for the convex splitting scheme at time $T = 1.0$ with different time steps are presented in Table 5.4, which goes well with the theoretical result of the unconditional energy stability for the scheme. Table 5.5 shows the proposed second order scheme (4.14) is indeed second order accurate in time. To obtain high order accuracy in both space and time, we choose $\mathcal{P}^k$ approximation for spatial discretization and the semi-implicit Runge–Kutta time marching method. Table 5.6 presents the L^2 and L^∞ errors and numerical orders of accuracy at time $T = 0.5$, which shows that the semi-implicit Runge–Kutta method coupled with $\mathcal{P}^k$ approximation gives a $(k + 1)$th order of accuracy for the PFC equation with degenerate mobility. The convergence rates of the multigrid solver are shown in Figure 5.2 and we can see a Δx-independent reduction in the residual for both $\mathcal{P}^1$ and $\mathcal{P}^2$ approximation, which suggests that the solver is of optimal complexity.

In the following long time simulation examples, we adopt different time steps to enhance the efficiency of the proposed time discretization methods, based on the evolution of energy. To show that the energy evolution is independent of time steps, we present in Figure 5.3 the energy trace of the numerical solution with different time steps.

Example 5.3 (long time simulation). In this example, we will show the long time characteristics of the PFC model with the random initial data on a square domain $[0, 128] \times [0, 128]$. The initial condition is the random perturbation around 0.07 with a fluctuation no larger than 0.07, i.e., $\phi^0_{i,j} = \bar{\phi} + \eta_{i,j}$, where $\bar{\phi} = 0.07$ and $\eta_{i,j}$ is a random number satisfying $-\bar{\phi} \leqslant \eta_{i,j} \leqslant \bar{\phi}$. The parameter ϵ in the PFC model is 0.025

TABLE 5.6
Accuracy test for PFC equation with degenerate mobility with third order semi-implicit Runge–Kutta method at $T = 0.5$. $\Delta t = 0.1\Delta x$.

	N	L^2 error	Order	L^∞ error	Order
$\mathcal{P}^1$	8	1.37E-02	–	6.12E-02	–
	16	3.42E-03	2.00	1.61E-02	1.93
	32	8.57E-04	2.00	4.08E-03	1.98
	64	2.14E-04	2.00	1.03E-03	1.98
$\mathcal{P}^2$	8	2.34E-03	–	1.07E-02	–
	16	2.42E-04	3.27	1.31E-03	3.03
	32	2.79E-05	3.11	1.59E-04	3.04
	64	3.40E-06	3.03	1.95E-05	3.02

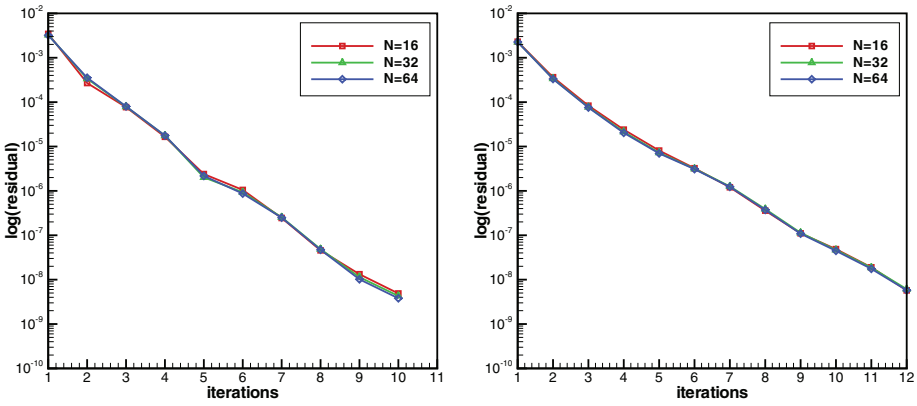

(a) $\mathcal{P}^1$ approximation (b) $\mathcal{P}^2$ approximation

FIG. 5.2. *Convergence rates of multigrid solver with $\mathcal{P}^1$ and $\mathcal{P}^2$ approximation for Example* 5.2.

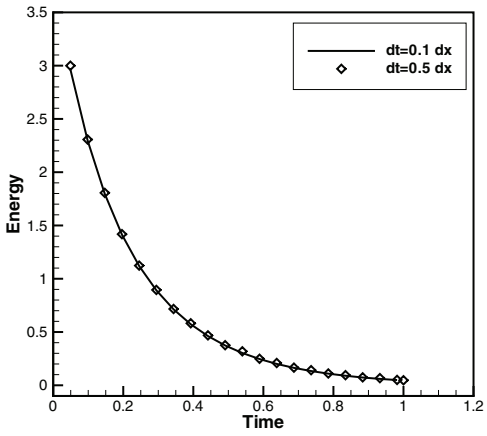

FIG. 5.3. *Energy trace of numerical solution for Example* 5.2 *with different time steps.*

and the periodic boundary condition is taken here. We consider the following cases for the mobility $M(\phi)$:

1. $M(\phi) = 1 - \phi^2$,
2. $M(\phi) = 1$, which is the maximum of the degenerate mobility.

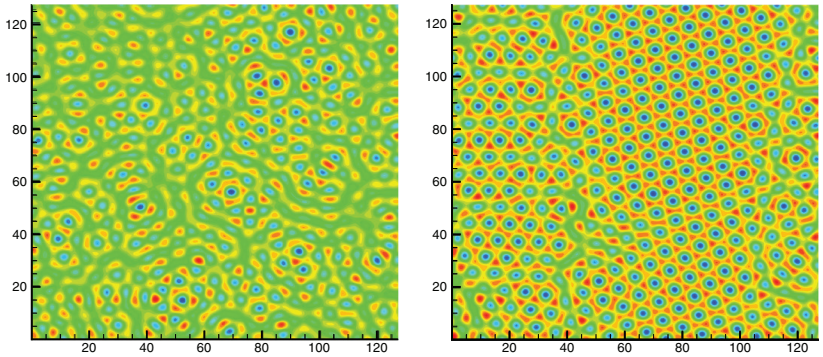

(a) $T = 400$ $\Delta t = 0.02$ (b) $T = 800$ $\Delta t = 0.1$

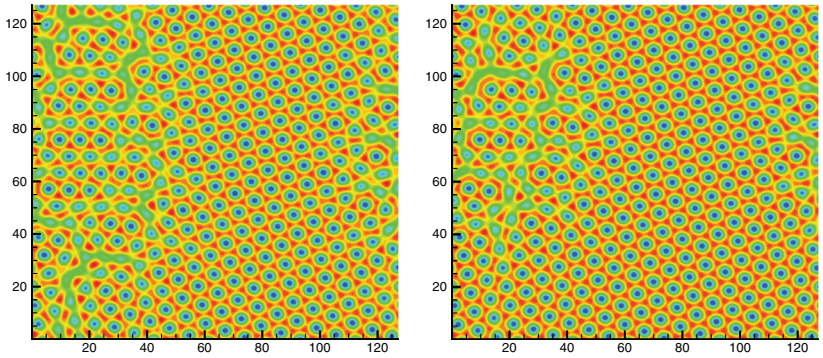

(c) $T = 1200$ $\Delta t = 0.5$ (d) $T = 2400$ $\Delta t = 3.0$

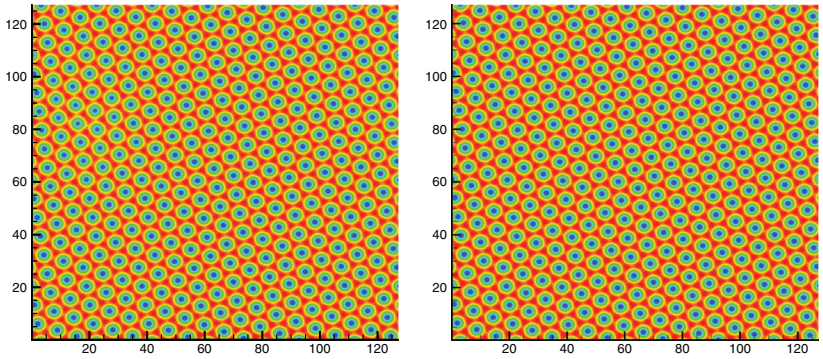

(e) $T = 4000$ $\Delta t = 5.0$ (f) $T = 10000$ $\Delta t = 10.0$

FIG. 5.4. *The time evolution of the PFC equation implemented with* $\mathcal{P}^2$ *elements for Example* 5.3 *with degenerate mobility* $M(\phi) = 1 - \phi^2$.

The computational parameters are the spatial discretization cell size $h = 128/N$ with $N = 256$ and the piecewise $\mathcal{P}^k$ polynomial basis with $k = 2$. For the PFC equation with degenerate mobility $M(\phi) = 1 - \phi^2$, the third order semi-implicit Runge–Kutta method is employed, while for the constant case, we apply the third order SDC time marching method.

Numerical results for these two different cases with different time steps are shown in Figures 5.4 and 5.5, which are qualitatively consistent with those presented in [11].

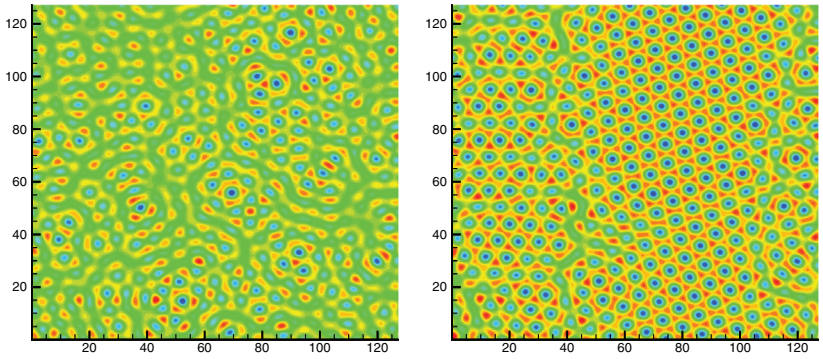

(a) $T = 400$ $\Delta t = 0.02$ (b) $T = 800$ $\Delta t = 0.1$

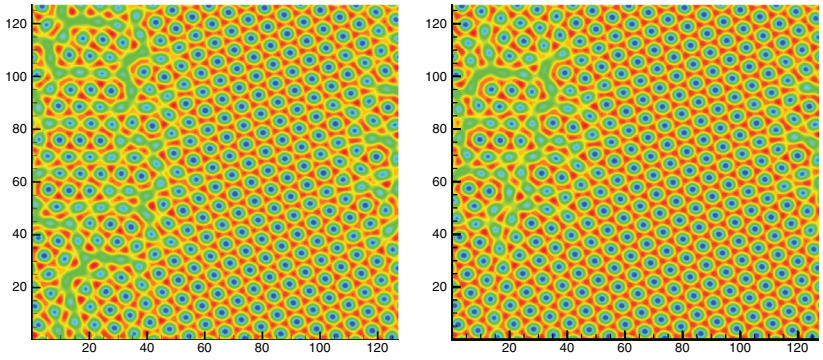

(c) $T = 1200$ $\Delta t = 0.5$ (d) $T = 2400$ $\Delta t = 3.0$

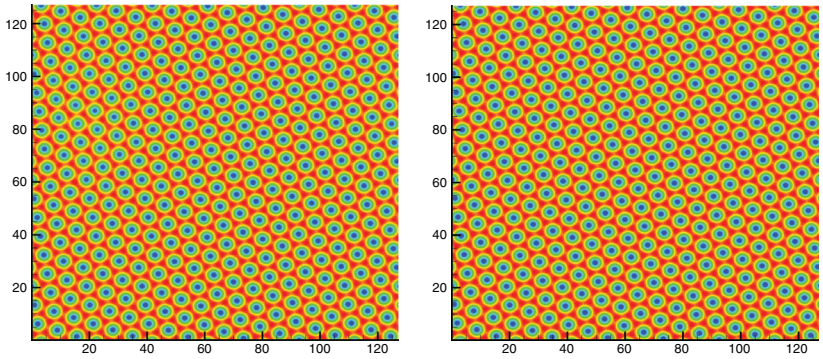

(e) $T = 4000$ $\Delta t = 5.0$ (f) $T = 10000$ $\Delta t = 10.0$

FIG. 5.5. *The time evolution of the PFC equation implemented with* $\mathcal{P}^2$ *elements for Example* 5.3 *with constant mobility* $M(\phi) = 1$.

Figures 5.6 and 5.7 show the discrete energy trace of the numerical solution. We can see that the energy is nonincreasing in time, which agrees with the theoretical result. At the early stage of dynamics of the PFC equation, the discrete energy decays quickly, and then the energy decays rather slowly. Based on these observations, we are motivated to use different time steps as presented in Figures 5.4 and 5.5.

Example 5.4 (growth of a polycrystal). This example presents the growth of a polycrystal in a supercooled liquid. To define the initial configuration we proceed as

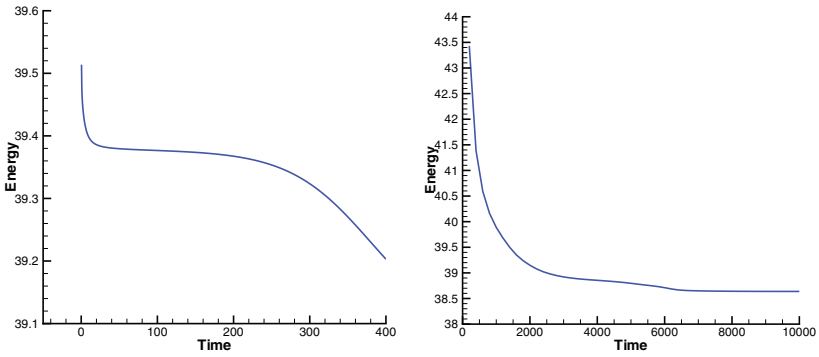

(a) $T = 400$ (b) $T = 10000$

FIG. 5.6. *Discrete energy trace of numerical solution for Example* 5.3 *with degenerate mobility* $M(\phi) = 1 - \phi^2$.

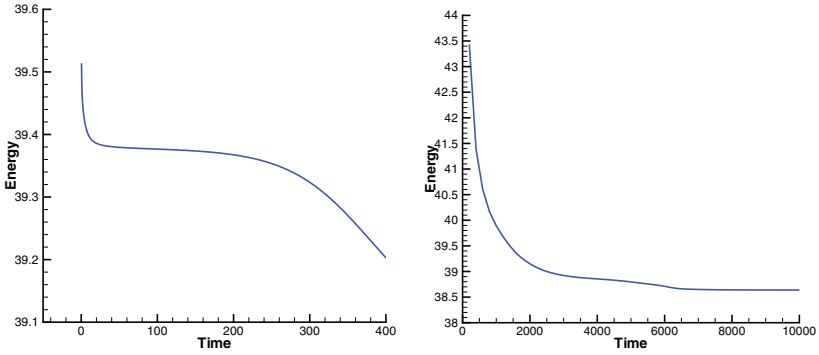

(a) $T = 400$ (b) $T = 10000$

FIG. 5.7. *Discrete energy trace of numerical solution for Example* 5.3 *with constant mobility* $M(\phi) = 1$.

follows: we first set all control variables to a constant value $\bar{\phi} = 0.285$, and then we modify this constant configuration by setting three perfect crystallites in three small square patches of the domain. The crystallites are defined as follows:

$$\phi(x_l, y_l) = \bar{\phi} + C\left[\cos\left(\frac{q}{\sqrt{3}}y_l\right)\cos(qx_l) - 0.5\cos\left(\frac{2q}{\sqrt{3}}y_l\right)\right], \tag{5.4}$$

where x_l and y_l define a local system of cartesian coordinates that is oriented with the crystallite lattice. Here, the local coordinates (x_l, y_l) are defined by an affine transformation of the global coordinates (x, y), which produces a rotation given by an angle α. Also, α are chosen as $-\frac{\pi}{4}$, 0, and $\frac{\pi}{4}$, respectively, to generate crystallite lattices with different orientations. We take the parameter $C = 0.446$ and $q = 0.66$.

The square domain is $(0, 804) \times (0, 804)$ with $\epsilon = 0.25$ and $M(\phi) = 1$. The periodic boundary condition is taken here. The computational parameters are the spatial discretization cell size $\Delta x = 804/N$ with $N = 512$ and the piecewise $\mathcal{P}^k$ polynomial basis with $k = 1$, and the second order SDC time temporal method. Numerical results with different time steps are shown in Figure 5.8, which shows statistically similar patterns in the numerical solution as those in [10]. Figure 5.9

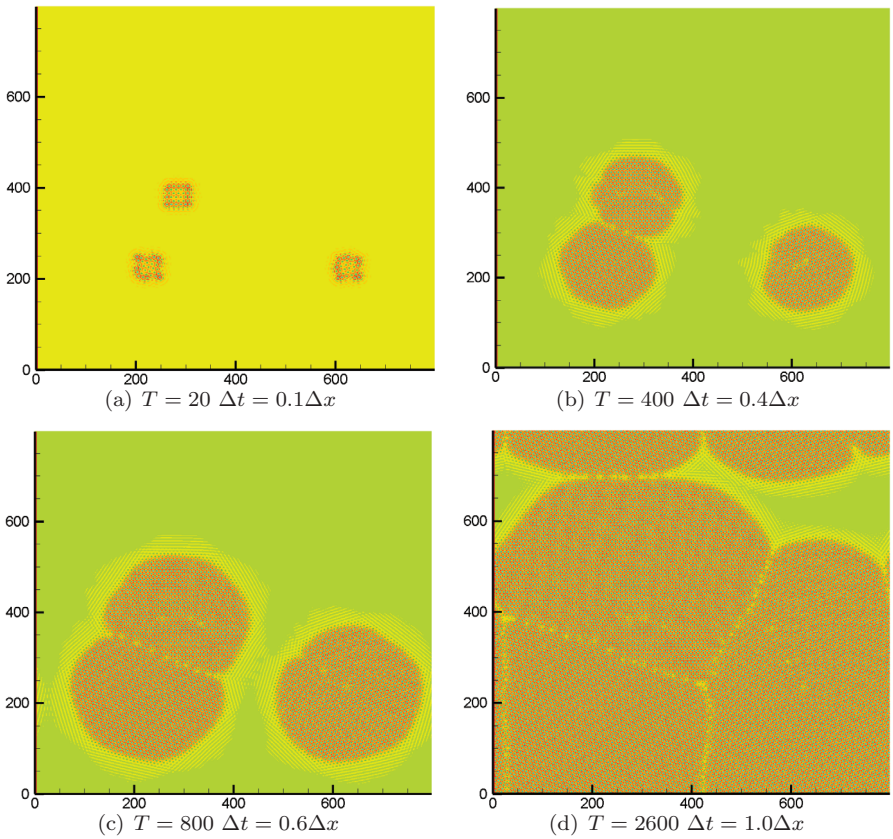

(a) $T = 20$ $\Delta t = 0.1\Delta x$ (b) $T = 400$ $\Delta t = 0.4\Delta x$

(c) $T = 800$ $\Delta t = 0.6\Delta x$ (d) $T = 2600$ $\Delta t = 1.0\Delta x$

FIG. 5.8. *The time evolution of the PFC equation implemented with* $\mathcal{P}^1$ *elements for Example* 5.4.

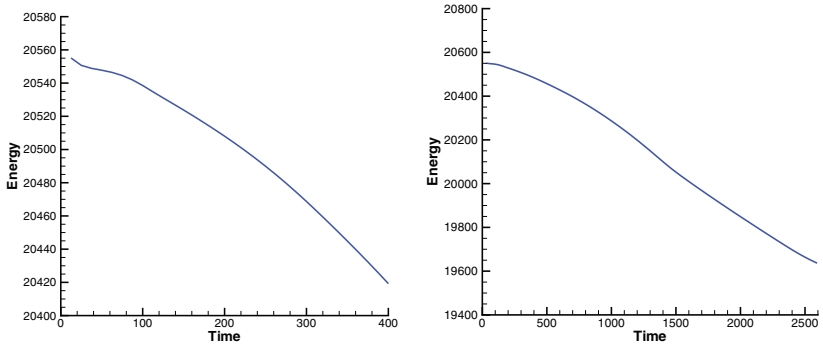

(a) $T = 400$ (b) $T = 2600$

FIG. 5.9. *Discrete energy trace of numerical solution for Example* 5.4.

shows the discrete energy trace of the numerical solution. We can see that the energy is nonincreasing in time, which agrees with the theoretical result.

6. Conclusion. In this paper, we developed a LDG method for the general nonlinear PFC equation and proved the energy stability for the semidiscrete scheme. To avoid the extremely small time step restriction of explicit methods, two convex split-

ting temporal discretization methods were employed, and the corresponding unconditional energy stabilities for the fully discrete schemes were presented. However, the convex splitting methods were only first or second order accurate in time. To achieve high order temporal accuracy, the SDC method and the semi-implicit Runge–Kutta method were adopted for the PFC equation with constant and degenerate mobility, respectively. With these proposed methods, the equations at the implicit time level were nonlinear and we employed an efficient nonlinear multigrid solver to solve the equations. Numerical experiments based on these proposed schemes were given to validate the theoretical results and to show the effectiveness of the spatial and temporal discretization methods for approximating the PFC equation.

REFERENCES

[1] S. Boscarino, F. Filbet, and G. Russo, *High order semi-implicit schemes for time dependent partial differential equations*, preprint.

[2] A. Brandt, *Multigrid techniques:* 1984 *Guide with Applications to Fluid Dynamics*, GMD-Studien 85, Gesellschaft für Mathematik und Datenverarbeitung mbH, St. Augustin, 1984.

[3] B. Cockburn and C. -W. Shu, *TVB Runge-Kutta local projection discontinuous Galerkin finite element method for conservation laws* II*: General framework*, Math. Comp., 52 (1989), pp. 411–435.

[4] B. Cockburn, S. -Y. Lin, and C. -W. Shu, *TVB Runge-Kutta local projection discontinuous Galerkin finite element method for conservation laws* III*: One dimensional systems*, J. Comput. Phys., 84 (1989), pp. 90–113.

[5] B. Cockburn, S. Hou, and C. -W. Shu, *The Runge-Kutta local projection discontinuous Galerkin finite element method for conservation laws* IV*: The multidimensional case*, Math. Comp., 54 (1990), pp. 545–581.

[6] B. Cockburn and C. -W. Shu, *The Runge-Kutta discontinuous Galerkin method for conservation laws* V*: Multidimensional systems*, J. Comput. Phys., 141 (1998), pp. 199–224.

[7] A. Dutt, L. Greengard, and V. Rokhlin, *Spectral deferred correction methods for ordinary differential equations*, BIT, 40 (2000), pp. 241–266.

[8] K. R. Elder, M. Katakowski, M. Haataja, and M. Grant, *Modeling elasticity in crystal growth*, Phys. Rev. Lett., 88 (2002), 245701.

[9] K. R. Elder and M. Grant, *Modeling elastic and plastic deformations in nonequilibrium processing using phase field crystal*, Phys. Rev. E, 68 (2003), 066703.

[10] H. Gomez and X. Nogueira, *An unconditionally energy-stable method for the phase field crystal equation*, Comput. Methods Appl. Mech. Engrg., 249 (2012), pp. 52–61.

[11] Z. Hu, S. M. Wise, C. Wang, and J. S. Lowengrub, *Stable and efficient finite-difference nonlinear-multigrid schemes for the phase field crystal equation*, J. Comput. Phys., 228 (2009), pp. 5323–5339.

[12] M. L. Minion, *Semi-implicit spectral deferred correction methods for ordinary differential equations*, Commun. Math. Sci., 1 (2003), pp. 471–500.

[13] N. Provatas, J. A. Dantzig, B. Athreya, P. Chan, P. Stefanovic, N. Goldenfeld, and K. R. Elder, *Using the phase field crystal method in the multiscale modeling of microstructure evolution*, JOM, 59 (2007), pp. 83.

[14] W. H. Reed and T. R. Hill, *Triangular Mesh Method for the Neutron Transport Equation*, Technical report LA-UR-73–479, Los Alamos Scientific Laboratory, Los Alamos, NM, 1973.

[15] J. Swift and P. C. Hohenberg, *Hydrodynamic fluctuations at the convective instability*, Phys. Rev. A, 15 (1977), pp. 319–328.

[16] S. M. Wise, C. Wang, and J. S. Lowengrub, *An energy-stable and convergent finite-difference scheme for the phase field crystal equation*, SIAM J. Numer. Anal., 44 (2009), pp. 2269–2288.

[17] Y. Xia, Y. Xu, and C. -W. Shu, *Efficient time discretization for local discontinuous Galerkin methods*, Discrete Contin. Dyn. Syst. Ser. B, 8 (2007), pp. 677–693.

[18] Y. Xia, *A fully discrete stable discontinuous Galerkin method for the thin film epitaxy problem without slope selection*, J. Comput. Phys., 280 (2015), pp. 248–260.

[19] Y. Xu and C. -W. Shu, *Local discontinuous Galerkin methods for high-order time-dependent partial differential equations*, Commun. Comput. Phys., 7 (2010), pp. 1–46.

[20] J. Yan and C. -W. Shu, *A local discontinuous Galerkin method for KdV type equations*, SIAM J. Numer. Anal., 40 (2002), pp. 769–791.